Stunting in infancy is associated with atypical activation of working memory and attention networks

Sobanawartiny Wijeakumar [a,b*], Samuel H. Forbes[c], Vincent A. Magnotta[d], Sean Deoni[e,f,g], Kiara Jackson[i], Vinay P. Singh[h], Madhuri Tiwari[h], Aarti Kumar[h] & John P. Spencer[i*]

a. School of Psychology, University of Nottingham, NG7 2RD, Nottingham, England, U.K.
b. Psychology, Faculty of Natural Sciences, University of Stirling, FK9 4LA, Stirling, Scotland, U.K.
c. Department of Psychology, Durham University, DH1 3LE, Durham, England, U.K.
d. Department of Radiology, University of Iowa, Iowa, U.S.A.
e. Maternal, Newborn, and Child Health Discovery & Tools, Bill & Melinda Gates Foundation, Seattle WA, USA
f. Advanced Baby Imaging Lab, New England Pediatric Institute of Neurodevelopment, Rhode Island Hospital, Providence RI, USA
g. Department of Pediatrics, Warren Alpert Medical School at Brown University, Providence RI, USA
h. Community Empowerment Lab, Lucknow, Uttar Pradesh, India.
i. School of Psychology, University of East Anglia, NR4 7TJ, Norwich, England U.K.

Corresponding authors:

Sobanawartiny Wijeakumar
B71
School of Psychology
University of Nottingham
NG7 2RD
United Kingdom
sobanawartiny.wijeakumar@nottingham.ac.uk

John P. Spencer
0.09 Lawrence Stenhouse
School of Psychology
University of East Anglia
NR4 7TJ
United Kingdom
j.spencer@uea.ac.uk

Classifications: Biological Sciences (Psychological and Cognitive Sciences)

Keywords: stunting; visual cognition; infancy

Summary

Stunting is associated with poor long-term cognitive, academic, and economic outcomes, yet the mechanisms through which stunting impacts cognition in early development remain unknown. In a first-ever neuroimaging study conducted in infants from rural India, we demonstrate that stunting impacts a critical, early-developing cognitive system – visual working memory (VWM). Stunted infants showed poor VWM performance and were easily distractible. Poor performance was associated with reduced engagement of the left anterior intraparietal sulcus (laIPS), a region involved in VWM maintenance, and greater suppression in the right temporo-parietal junction, a region involved in attentional shifting. When assessed one year later, stunted infants had lower problem-solving scores, while normal height infants with greater laIPS activation showed higher problem-solving scores. Finally, short-for-age infants with poor physical growth indices but good VWM performance showed more positive outcomes suggesting that intervention efforts should focus on improving working memory and reducing distractibility in infancy.

Introduction

Stunting or linear growth faltering often begins in utero and continues to unfold within the first 1000 days of a child's life. It is caused by a combination of factors such as poor nutrition, inadequate maternal health, exposure to infectious diseases and unhygienic environments, caregiver neglect, and lack of stimulation. Stunting impacts approximately 150 million children under the age of five worldwide (UNICEF/WHO/World Bank Group Joint Child Malnutrition Estimates 2021 Edition). In developing countries, stunting is associated with late enrolment in school and reduced educational attainment[1,2]. These deleterious effects typically continue into adulthood leading to a 20% reduction in adult income[3], 1.4% loss in economic productivity[4], and a total economic cost of $176.8 million per birth cohort[5]. Thus, stunting has an adverse impact at the individual, household, and community levels, eventually perpetuating an inter-generational cycle of poverty and undernutrition.

Persistent stunting that begins early in life has a particularly strong impact on cognitive outcomes in later childhood. In a meta-analytic study conducted across 29 low-to-middle-income countries, a one-unit increase in height-adjusted z-scores (HAZ) for children under 2 years of age was associated with a 0.22 standard deviation increase in cognition between 5 and 11 years of age[6]. Given this early impact, it is critical to understand how stunting affects neurocognitive mechanisms in the first year of life. Using portable neuroimaging techniques very early in development may be a powerful approach to address this issue. To date, only one neuroimaging study has investigated the impact of stunting on brain function in infancy[7]. This study examined growth measures and brain functional connectivity using electroencephalography in two groups of urban Bangladeshi children: a younger cohort aged 6 months and an older cohort aged 36 months. In the older cohort, there was an association between lower HAZ scores, greater brain functional connectivity in the theta and beta frequency bands, and a reduction in children's IQ scores at 48 months of age. Notably, the study did not find a link between HAZ scores and brain function in the younger 6-month-old cohort, nor did the study clarify how stunting might impact cognitive functions in the first year of life.

What cognitive systems are likely to be impacted by stunting in early development? One potential target is visual working memory (VWM), a critical cognitive system that emerges within months after birth, develops rapidly across early childhood and is susceptible to early risk factors[8]. Early in development, rich explorative play can enhance VWM and attentional networks leading to visual familiarity with objects and better retention of object-label associations which is important for word-learning and vocabulary development[9]. VWM processing is also predictive of individual differences in global fluid intelligence[10] and academic outcomes[11]. For instance, WM processing has been linked to vocabulary scores[12], non-symbolic scores[12], comprehension[13], and mathematics abilities[14] in primary school and later school years. Given these predictive associations between VWM processing and later academic achievements and the insidious impact of stunting on cognitive and academic outcomes, it is important to examine VWM processing in infants at risk of stunted development.

How might VWM be assessed in infancy? One option is to use a preferential looking task to measure looking behaviour and VWM function[15–17]. In this task, infants are presented with two flashing side-by-side displays of colored squares (Fig. 1a and 1b). On the 'unchanging' side, the colors of the squares remain the same after each flash, while on the 'changing' side, there is a change in the color of one square after each flash. If infants can maintain the colors on the unchanging display in VWM during the delay, they should lose interest in this display, releasing fixation to visually explore the 'changing' display. Here, they should detect the change and sustain looking to this display, leading to a strong *change preference* (CP) score – a high proportion of looking to the changing side.

Previous work has shown that CP scores vary with the number of presented items (VWM load) [15,18,19] and there is a developmental improvement in VWM capacity with age. Ross-Sheehy et al. (2003) showed that 6.5-month-old infants demonstrate greater-than-chance CP scores with a VWM load of one item, while older infants of 10 and 13 months of age showed greater-than-chance CP scores for VWM loads of two and three items[15]. Similarly, both 6-month-old and 8-month-old infants show a preference for one complex object, but only 8-month-old infants display a preference for two complex objects[18].

Critically, recent neuroimaging work has shown that infants engaging with the preferential looking VWM task modulate a fronto-temporo-parietal VWM network typically activated in adults. This work used functional near-infrared spectroscopy (fNIRS) to measure brain function in urban US infants[16]. Results revealed that visual exploratory measures were associated with activation of the dorsolateral prefrontal cortex (DLPFC). Further, infants showed task-dependent modulation of the anterior intraparietal sulcus (aIPS) and the temporoparietal junction (TPJ)[20,21]. In adult studies, aIPS, a part of the dorsal attention network, is associated with maintaining working memory representations[22,23], while TPJ, a part of the ventral attention network, is typically suppressed in working memory tasks reflecting suppression of attentional shifts away from task goals[20].

In the current study, we used the same VWM task and fNIRS neuroimaging methods to conduct the first-ever community-based study investigating the impact of stunting on neurocognitive function in infants in rural India. We situated the study in a low-resource setting in Uttar Pradesh; a recent initiative investigating child growth failures under the National Nutrition Mission reported that 97.3% of the state's districts fell within the high tertile for stunting[24]. Our motivation for choosing this location was further justified by findings in a sample of children in Shivgarh, Uttar Pradesh: children from lower socioeconomic status families showed poorer VWM performance and distractor suppression in inferior frontal gyrus (IFG), a region in the VWM network[17]. Thus, in the current study, we recruited 6- and 9-month-old infants from high and low socioeconomic families and followed them for two years. We included both ages to assess whether this cohort would demonstrate shifts in behaviour between the ages of 6 and 9 months in line with previous work[18,19]. Alternatively, studying these two age groups might reveal delays in behaviour and/or brain function relative to urban US infants. Portable eye-tracking and video recordings were used to examine how infants visually explored the VWM task. fNIRS was used to measure brain function in the infants as they engaged with the task (Fig. 1c). Growth measures were collected at multiple time-points across the two years to determine stunting status and growth rate. Finally, the Ages and Stages Questionnaire (ASQ) was administered in the second year to examine the impact of stunting and VWM function on later cognitive outcomes.

We focused on three central questions. First, we inquired whether stunting was associated with poorer VWM performance in the first year of life. Second, we asked how stunting impacted brain function - do stunted infants differentially engage the fronto-parietal VWM network compared to normal height infants? Finally, we investigated whether VWM performance and brain function in the first year were related to cognitive outcomes a year later, and how these outcomes were modulated by stunting.

Results

What is the impact of stunting on VWM behaviour in infancy? We asked whether stunting was associated with poorer VWM performance in the first year of life. To address this question, we analyzed CP scores using a linear model with age (6 and 9 months), load (1, 2, or 3 coloured items on each display), HAZ score (height-for-age z-score), and total looking time (TLT) as predictors. We included TLT in the model because it was not correlated with CP and captured

a significant proportion of variance in the CP scores. Furthermore, CP scores were calculated over a critical time window (see Methods) while TLT was calculated across the full duration of the trial. All interactions among predictor variables were included. There were significant main effects of load ($F(1,639) = 6.14$, $p = 0.013$), TLT ($F(1,639) = 6.86$, $p = 0.009$), and HAZ ($F(1,639) = 5.62$, $p = 0.018$) on CP scores (see Fig. 1d). As in previous studies conducted with western samples, CP scores declined as the load increased. Further, infants with higher CP scores explored the displays for longer durations. Critically, a decrease in HAZ scores was associated with lower CP scores, reflecting poorer VWM performance in infancy.

There were also significant two-way interactions between HAZ and load ($F(1,639) = 5.42$, $p = 0.02$), load and TLT ($F(1,639) = 6.30$, $p = 0.012$), and HAZ and TLT ($F(1,639) = 5.95$, $p = 0.015$); these interactions were subsumed by a significant three-way interaction between HAZ, load, and TLT ($F(1,639) = 5.43$, $p = 0.02$). Follow-up tests revealed a robust interaction between HAZ and TLT at the low load ($F(1,211) = 6.68$, $p = 0.01$) with no significant interactions at the medium and high loads (all $p > 0.05$). At the low load, increasing HAZ scores were associated with increasing CP scores in infants with longer looking durations (see Supplementary Fig. 1a). By contrast, infants who failed to sustain longer looking durations had difficulty detecting the changing side with CP scores near chance levels (i.e., 0.50). Finally, there was a significant two-way interaction between age and HAZ ($F(1,639) = 4.24$, $p = 0.04$; see Supplementary Fig. 1b). This effect appeared to be more strongly driven by 6-month-olds compared to 9-month-olds. Specifically, 6-month-olds showed a strong linear relationship between CP scores and HAZ scores, with normal height infants showing higher CP scores. By contrast, 9-month-old infants did not demonstrate a linear relationship between CP scores and HAZ scores. They did better in the task overall with some infants showing CP scores greater than chance levels.

Is the canonical VWM brain network engaged in infants from rural India? Our next goal was to examine infants' brain function as they engaged in the VWM task. Co-registered beta maps from individual-level general linear modelling (see methods and materials) were entered into a group-level linear mixed effects model with load (1, 2, 3), chromophore (HbO and HbR), CP scores, age, and HAZ scores as predictors. The model also included a random intercept for each participant to account for individual level variance. We focused on significant main effects and interactions that included chromophore, as HbO and HbR are typically anti-correlated. Group-level clusters with significant effects following familywise correction (see methods and materials) are shown in Table 1. We discuss each set of effects below.

Infants engaged a canonical fronto-temporo-parietal VWM network while visually exploring the displays in the preferential looking VWM task. Critically, we replicated a finding from our prior study in the same population: there was a significant interaction between CP score and chromophore in the right IFG (rIFG). As shown in Figure 2, infants with weak or supressed activation in rIFG (i.e., lower HbO concentration/higher HbR concentration) showed higher CP scores. In previous work, greater IFG activation has been associated with poorer distractor suppression[17,25]. Thus, our findings suggest that infants with better VWM scores were able to suppress looks to the unchanging side via rIFG suppression. On the other hand, infants who activated rIFG showed poor distractor suppression, more frequent looks to the unchanging side, and lower CP scores.

One main effect and multiple interaction effects were observed in different clusters of the left aIPS (laIPS; see Table 1), a part of the dorsal attention network engaged during VWM maintenance. We discuss the developmental and performance-related effects observed in laIPS first; stunting-related effects are discussed below. A main effect of chromophore was observed in the anterior portion of the laIPS, with the canonical pattern of increasing HbO and decreasing HbR concentrations (see left panel in Figure 3a and blue cluster on brain image). An interaction

between age and chromophore was also observed in an adjoining laIPS cluster (see right panels in Figure 3a and green cluster on brain image). Specifically, 6-month-old infants showed greater laIPS activation compared to 9-month-old infants. Considered together with the main effect, the interaction between age and chromophore suggests refinement of laIPS activation with development.

This pattern was qualified by the significant interaction between age, CP score, and chromophore in the inferior portion of the laIPS shown in Figure 3b (see red cluster). Here, 9-month-old infants who performed poorly in the VWM task showed engagement of laIPS, while higher-performing 9-month-olds did not. Low-performing 6-month-old infants, by contrast, showed suppression in this laIPS cluster. Thus, the overall pattern shown in Figure 3 suggests that laIPS activation becomes more refined with age and enhanced performance in the task. There is also evidence that the youngest, low-performing infants showed a different pattern – suppression – in an inferior portion of the laIPS.

Before turning to the stunting-related effects, we note there was a significant interaction between load, CP score, and chromophore in the right frontal eye fields (rFEF; see Table 1). Activation in this region is associated with preparation and control of eye-movements and gaze[26,27]. We generally found suppression of rFEF for both higher- and lower-performing infants (see Supplementary Figure 2); however, this effect was inconsistent as a function of load. It is possible that the lack of a clear pattern with increasing load reflects ongoing functional refinement in this region relative to infants' improving visual exploratory abilities.

What is the impact of stunting on brain function? The findings above confirm that infants from rural India engaged a canonical VWM brain network and replicated prior findings from this population. Next, we asked how stunting impacted brain function in infancy. We found that stunting impacted activation in three regions (see Table 1): (1) laIPS, a key region in the dorsal attention network, (2) rTPJ, a key region of the ventral attention network, and (3) lDLPFC, an area involved in top-down control of processing in posterior regions of the brain.

A significant three-way interaction between HAZ, load, and chromophore was observed in a superior laIPS cluster (see lavender cluster in Figure 4a). Here, normal height infants engaged laIPS in a load-dependent manner consistent with infants from an urban US sample with a decrease in activation at higher loads[28]. By contrast, stunted infants did not modulate laIPS activation with increasing load, although they showed some evidence of greater suppression of laIPS at the low load (i.e., negative HbO and positive HbR).

Activation in laIPS was also related to behavioural performance and stunting through a four-way interaction between HAZ, age, CP score, and chromophore in a more inferior laIPS cluster (see white cluster in Figure 4b). Both 6- and 9-month-old normal height infants showed robust activation in this laIPS cluster, with lower activation for higher-performing infants. This is consistent with results from Figure 3 suggesting a refinement in laIPS activation with age and enhanced task performance. By contrast, stunted infants showed much weaker activation in this cluster. The one exception was 6-month-old stunted infants who performed better in the VWM task; these infants showed modest laIPS activation.

The next finding is shown in Figure 5: suppression in rTPJ was related to behavioural performance through a three-way interaction between HAZ, CP score, and chromophore. In normal height infants, greater rTPJ suppression was associated with better CP scores. This finding is consistent with previous adult studies showing rTPJ suppression (along with laIPS activation) during VWM processing to prevent shifts in attention away from task goals[20]. In contrast, in stunted infants, greater rTPJ suppression was associated with poorer CP scores suggesting that stunted children tended to maintain attention to the unchanging side resulting in rTPJ suppression and poor CP scores.

Finally, a three-way interaction between HAZ, age, and chromophore was observed in lDLPFC (see Figure 6). This interaction was driven by increased lDLPFC activation in normal height 6-month-olds and stunted 9-month-olds. Evidence suggests that the DLPFC is often engaged in working memory tasks to support processing in the parietal cortex early in development and during demanding working memory tasks[29]. Our findings suggest, therefore, that normal height 6-month-olds and stunted 9-month-olds recruited this frontal area in support of their VWM performance. We note that this is the one brain region that showed robust activation in stunted 9-month-old infants, some of whom successfully detected the changing side. Thus, the delayed recruitment of this frontal region may be adaptive for these infants.

Does stunting impact longer-term cognitive outcomes? As a final question, we investigated whether stunting, behavioural performance, and associated brain function in the first year of life were linked to cognitive outcomes one year later. In an initial linear model, we asked whether higher cognitive outcome scores in year 2 (problem-solving score from the ASQ; see methods and materials) were associated with CP in year 1 and physical growth measures. For the physical growth measures, we included HAZ (the intercept from our growth model; see materials and methods) and a linear growth term (HAZ-L), which captured change in HAZ over time, as predictors.

Results revealed a significant interaction between HAZ and HAZ-L in predicting problem-solving scores in year 2 ($F(1,164) = 4.30$, $p = 0.04$). This effect was subsumed by a significant three-way interaction between CP, HAZ, and HAZ-L ($F(1,164) = 4.29$, $p = 0.04$). As shown in Fig. 7a, normal height infants with higher linear growth had better outcomes in year 2. By contrast, normal height infants with lower linear growth fared poorer, except for infants with higher CP scores in year 1. These infants with higher CP scores showed good problem-solving scores in year 2. This finding suggests that VWM abilities in infancy might be protective against cognitive deficits associated with poor linear growth. In general, stunted infants showed poorer problem-solving scores in year 2.

Next, we asked whether the load-dependent patterns of activation observed in laIPS (see Figure 4a) predicted cognitive outcomes one year later. We ran separate models for HbO and HbR concentrations. Even though normal height infants elicited greatest activation at the low load, we did not observe any associations with the problem-solving score from this condition. However, we found a significant main effect of HbR concentration in laIPS at the medium load ($t(167) = -1.95$, $p = 0.05$): greater laIPS activation (i.e., negative HbR concentration) was associated with better problem-solving scores in year 2. As shown in Fig. 7b, there was also a significant interaction between HbR concentration in laIPS and HAZ scores ($t(167) = -2.46$, $p = 0.015$). In normal height infants, greater laIPS activation (i.e., negative HbR concentration) was associated with better problem-solving scores in year 2. Follow-up tests showed no robust associations between brain activation and problem-solving scores for stunted infants ($p > .05$).

Discussion

Stunting in the first 1000 days is associated with poor cognitive, academic, and economic outcomes in later life, yet the neurocognitive mechanisms underlying these relationships early in development are unknown. We hypothesized that stunting in infancy might impact early emerging cognitive systems such as VWM, a critical system that is predictive of individual differences in cognitive function and academic outcomes. Toward this end, we examined how stunting impacts VWM performance and brain function in the first year in a large sample of infants from rural India; we also examined cognitive outcomes one year later.

Consistent with findings from western settings, behavioural performance in the VWM task declined with increasing load[15,28]. Further, infants in this study engaged key hubs in the attention and VWM networks[30] such as rIFG, laIPS, and rTPJ as a function of VWM load and task-related performance. We also replicated a critical finding from our prior work in this population: infants who sustained longer looking to the changing side (greater CP scores) showed suppression in rIFG[17]. The inferior frontal junction is purported to act as a switching hub between the dorsal and ventral attention networks, with suppression implying less frequent switching between top-down goal-driven attention and bottom-up re-orienting of attention to salient/distracting stimuli[31]. We suggest that infants who sustained longer looking towards the changing side and showed better VWM performance, infrequently re-oriented attention to the unchanging side via IFG suppression. Increased frontal activation has also been linked to processing and storage of irrelevant distractor information in visual and spatial working memory tasks in children[32]. Thus, in the current study, greater rIFG activation in infants with poorer CP scores might also reflect processing of information from the distracting, unchanging side.

Previous studies with children and adults have shown that active working memory maintenance is associated with *bilateral* posterior parietal activation[20,21,23,33]. Further, parietal lateralization has been linked to the type of working memory used, with verbal working memory activating left parietal cortex and some studies showing greater involvement of right parietal cortex in visuo-spatial working memory[34]. In the current study, *only left* aIPS was engaged across multiple effects of age, load, chromophore, CP score and HAZ in infants suggesting a key role for this brain region in VWM processing. This is consistent with evidence from an urban US sample which revealed robust relationships between performance in the preferential looking VWM task and activation in the left hemisphere in infancy[28]. Environmental/contextual differences might explain the emergence of lateralized activation in the first year of life. For example, bilingual language, compared to monolingual language exposure in infants has been associated with bilateral recruitment of the frontal cortex during a non-linguistic attentional orienting task[35].

We also replicated another key effect from our prior study of urban US infants: normal height infants showed a load-dependent modulation in the laIPS with high activation at a low load and lower activation at higher loads. This pattern is consistent with similar effects in 3- and 4-year-old children[36] as well as aging adults[37]. Interestingly, this pattern contrasts with findings from adults; increasing VWM load is associated with increasing aIPS activation until a capacity limit is met; this is followed by an asymptote in brain activation[33,38,39]. Collectively, these findings suggest that at high loads, infants, children, and aging adults fail to maintain a near-capacity number of items (and an asymptotic level of brain activity). How, then, were some infants able to show above-chance levels of responding at the medium and high loads? On some of these trials, infants start visual exploration on the changing side. Detection of novelty in this case does not require robust working memory ability as there is a change after each flash. Thus, it is possible that some infants show above-chance responding because they started on the changing side, detected novelty, and this novelty sustains looking to this display[40].

We observed a refinement of laIPS activation with age and enhanced VWM performance. Specifically, 6-month-olds and low-performing 9-month-olds showed a greater extent of laIPS engagement. Moreover, in normal height children (compared to stunted infants), both age groups showed greater laIPS activation in lower-performing infants. These findings are novel and suggest a refinement of laIPS activation between 6 and 9 months in infants from rural India consistent with behavioural evidence of a change in VWM capacity between these ages in urban infants[28]. The extent of spatial refinement of laIPS activation

underscores the precision of the image reconstruction techniques we used (for a comparison to a channel-based fNIRS approach, see Supplementary materials).

The present study also revealed – for the first time – how stunting impacts looking behaviour. We found that stunted infants showed a poorer ability to detect and stay fixated on the changing side. The linear association between stunting status and CP scores was stronger in 6-month-old infants compared to 9-month-old infants suggesting that stunting-related impact on VWM processing might be mitigated with age. However, our brain imaging results imply otherwise. Stunting modulated activation in laIPS, rTPJ, and lDLPFC – key regions in the canonical fronto-temporo-parietal VWM network.

Unlike normal height infants, stunted infants more consistently showed weak activation in the laIPS – only high-performing 6-month-olds showed robust engagement of this brain region. In the absence of active laIPS engagement, how did some stunted 9-month-olds achieve above-chance performance? Our findings suggest that these infants recruited the lDLPFC, a region involved in the top-down modulation of processing in posterior parietal cortex. Thus, while 9-month-old normal height infants engaged laIPS to achieve sustained looking to the changing side, stunted 9-month-old infants might have engaged the frontal cortex to compensate for weak activation in laIPS. Notably, this pattern of dependence on frontal cortex activation was also observed in younger normal height infants. Taken together, our findings suggest that stunting status might be associated with impairments or delays in the functional activation of the VWM network.

Stunting status also selectively modulated rTPJ function. rTPJ is thought to act as a 'circuit-breaker' with greater activation associated with bottom-up reorienting of attention away from ongoing task-related processes and towards salient and/or irrelevant stimuli[20,21,41,42]. In VWM processing in adults, increasing VWM load is associated with increased laIPS activation and rTPJ suppression[20]. In agreement with this evidence, we found that normal height infants who showed better VWM performance and less distractibility engaged laIPS to successfully maintain representations of the items and supressed rTPJ to prevent frequent re-orientation of attention. On the other hand, in stunted infants, rTPJ suppression was associated with poor CP scores suggesting some of these infants might have gotten 'stuck' on the unchanging side.

As a final question, we asked whether these neurocognitive patterns impacted cognitive outcomes one year later. Our findings suggest that VWM function might act as a protective factor against deficits in more complex cognitive functions in later years, consistent with evidence showing that VWM function in infancy is a reliable predictor of cognitive outcomes 11 years later[43]. Concretely, at-risk infants with low height-for-age scores in infancy and lower linear growth from the first to the second year of life showed better problem-solving scores in year 2 if they had good VWM performance in year 1. We then asked whether laIPS activation in infancy was linked to better cognitive outcomes in year 2. Interestingly, normal height infants with greater laIPS activation in year 1 demonstrated higher cognitive scores in year 2.

It is important to contextualize these findings given that multiple factors may promote healthy VWM processing in the first year of life (see [44] for a review of biophysiological pathways impacted by poverty). Normal height infants might be reared in higher-resource homes with access to more cognitive materials and activities compared to stunted infants. Moreover, exposure to less stressful environments may promote opportunities for rich quantity and quality of explorative play leading to typical, healthy development of attention and VWM networks. Prior work from our group showed that parent-reported frequency of stressful life events was predictive of left parietal cortex engagement during a VWM task in low-performing pre-school children in Scotland[33]. Stunted children might also be exposed to living conditions with poor sanitisation, poor hygiene, pathogen exposure, and environmental contaminants leading to chronic infections and malnutrition. Resulting general malaise or sickness could lead

to diminished opportunities for explorative play and social learning impacting cognitive development in the first year of life. All these conditions could also lead to anatomical differences in brain structure and connectivity as well as reduced cortical activity, eventually affecting VWM and attention processing pathways.

Our findings are consistent with studies suggesting that stunted children show longer-term working memory deficits. For example, Walker et al. (2005) showed that stunting in the first 2 years of life was associated with poor performance in visual and spatial working memory function in 17- to 18-year-old adolescents in Jamaica[2]. Similarly, Kar et al. (2008) found that malnourished children across the age-groups of 5-7 years and 8-10 years in India showed poorer performance on a working memory task compared to adequately nourished children in these age-groups[45]. The current study makes a unique contribution to this body of work by using neuroimaging tools to study the most at-risk infants globally, demonstrating that such tools can be successfully deployed to investigate and identify neurocognitive mechanisms in rural settings[46,47]. We show that stunting impacts looking behaviour and is associated with modulation of neural activity in key hubs of the VWM and attention brain networks and, further, that these neurocognitive patterns are associated with later cognitive outcomes. Our findings also paint a picture of hope in that better VWM function in infancy may confer some neurocognitive protection, at least for short-for-age infants. Given that prior work suggests visual cognition can be enhanced via caregiver-based interventions[48], this could provide an avenue for future efforts to boost VWM function in infancy before stunting-related cognitive deficits take hold.

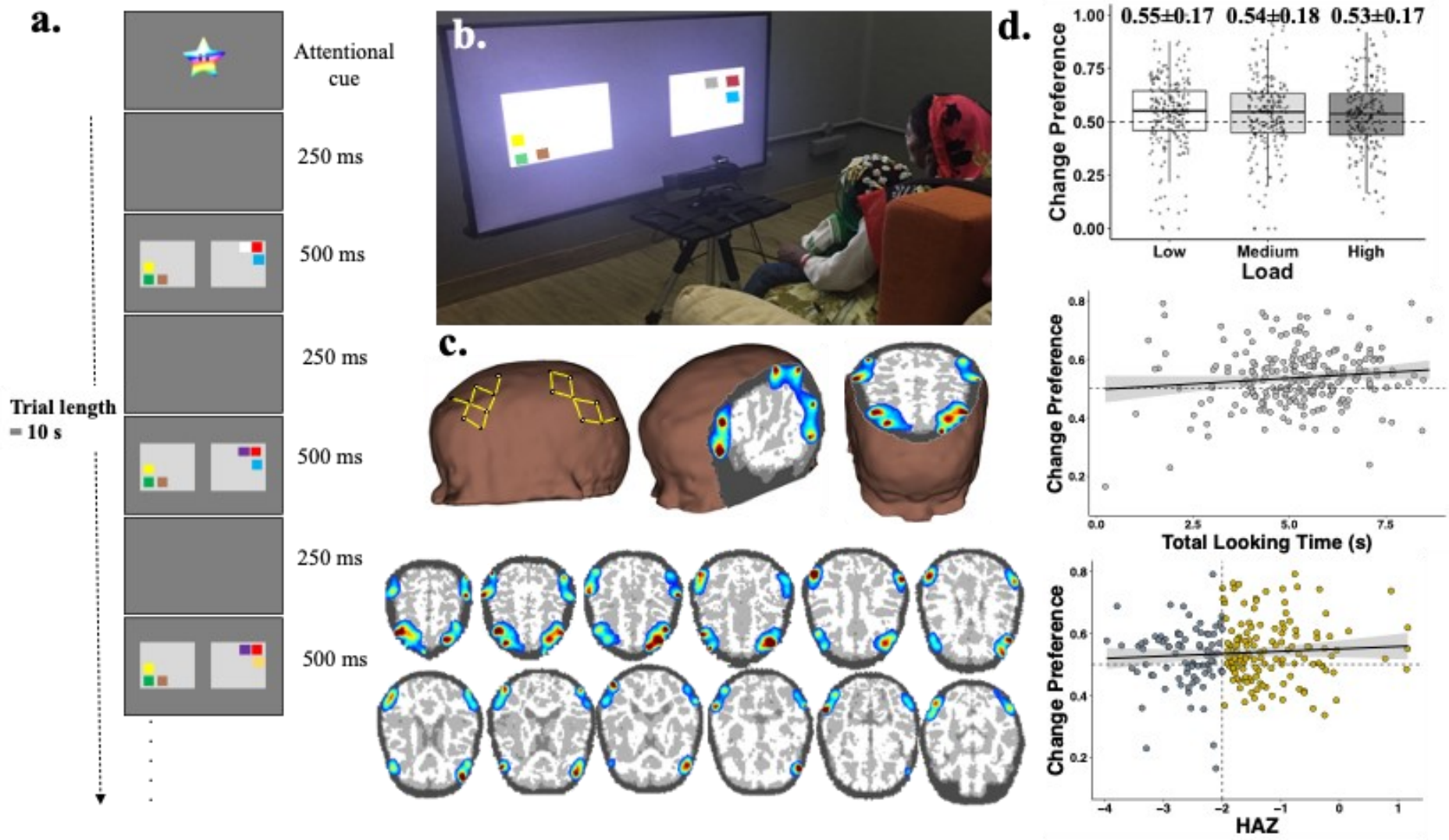

Figure 1. (a) A trial of length 10 s of the preferential looking VWM task. During the 10s trial, alternating blank displays for 250ms are followed by 'on' displays of colored squared for 500ms (i.e., 250ms, 500ms, 250ms, 500ms…for 10s). (b) Exemplar of infant engaging with the task and wearing the fNIRS cap as the

child sits on the mother's lap. (c) Top left image shows probe geometry covering the frontal, temporal and parietal cortices. Middle and right panels show sagittal and axial slice of photo migration results. Bottom panel shows superior (top) to inferior (bottom) axial slices of photon migration results. Hotter colors indicate stronger signal sensitivity. (d) Main effects from the analysis of change preference scores showing modulation over memory load (box plot in top panel shows median and SD [values shown] with lower and upper hinges corresponding to the first and third quartiles), total looking time (scatter plot in middle panel), and height-for-age z-scores (HAZ, scatter plot in lower panel). Colors in lower panel reflect typical cut-off scores used to identify stunted individuals (z-scores < -2) with grey showing stunted infants.

Effect	Region of interest	Size (mm^3)	Centre of mass coordinates		
			x	y	z
CP x Chromophore	Right inferior frontal gyrus (rIFG)	424	46.3	-154.2	142.2
Chromophore	Left anterior intraparietal sulcus (laIPS)	626	144.7	-103.8	181.6
Age x Chromophore	Left anterior intraparietal sulcus (laIPS)	400	138.1	-97	186.3
Age x CP x Chromophore	Left anterior intraparietal sulcus (laIPS)	354	155.5	-87.5	169.9
HAZ x Load x Chromophore	Left anterior intraparietal sulcus (laIPS)	562	139.1	-91.3	182.7
HAZ x Age x CP x Chromophore	Left anterior intraparietal sulcus (laIPS)	328	143.2	-103.5	181
HAZ x CP x Chromophore	Right temporo-parietal junction (rTPJ)	541	44	-80.7	152.1
HAZ x Age x Chromophore	Left dorsolateral prefrontal cortex (lDLPFC)	593	127.6	-162.7	171.5
Load x CP x Chromophore	Right frontal eye fields (rFEF)	603	74.6	-146.6	183.5

Table 1. Significant clusters of brain function engaged during the preferential looking task obtained from linear mixed-effects modelling. Note that significance was determined using familywise correction with voxel-wise $p = 0.01$, voxel threshold = 278 and alpha = 0.05.

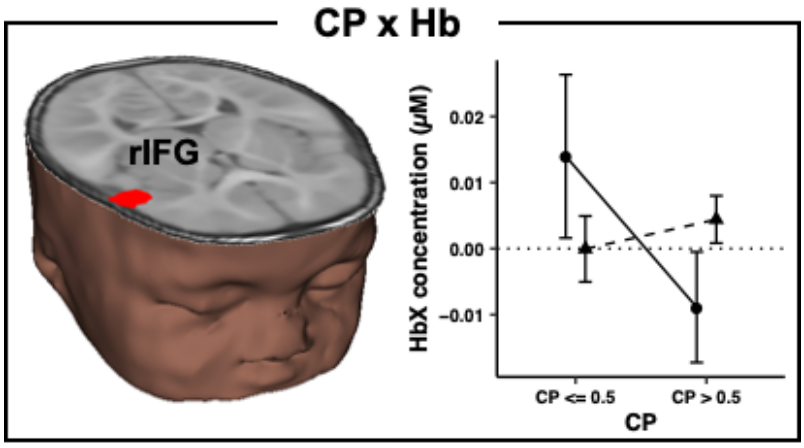

Figure 2. Brain image shows interaction between CP score and chromophore in right inferior frontal gyrus (rIFG; see red cluster in brain inset). Right panel shows mean ± SE HbO (solid circle) and HbR (dashed triangles) concentration across the hemodynamic time window (0-20s) for infants with CP scores less then chance (<=0.5) and CP scores greater than chance.

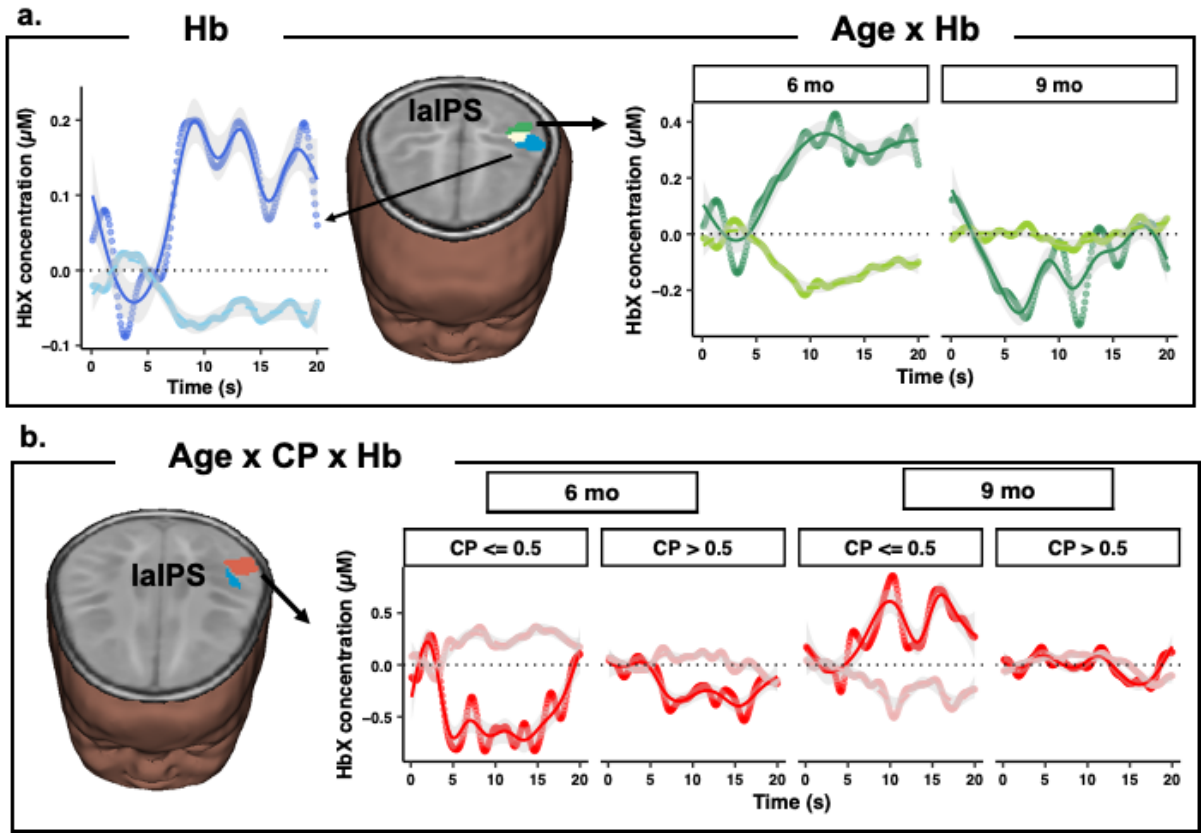

Figure 3. (a) Brain image shows location of main effect of chromophore (blue), interaction between age and chromophore (green), and overlap (white) in laIPS. Average time-series plots show HbO concentration in dark blue and HbR concentration in light blue for main effect of chromophore (left panel). Average time-series plots show HbO concentration in dark green and HbR concentration in light green for interaction between age and chromophore (right panel). We show data across the total hemodynamic time window (0-20s) with 0 = trial onset and 10s = trial offset. (b) Brain image shows location of interaction between age, CP score, and chromophore (red) close to the main effect of chromophore (blue). Average time-series plots showing HbO concentration in red and HbR concentration in light red for interaction between age, CP score, and chromophore (right panel). We show data for 6-month-old and 9-month-old infants with CP scores less then chance (<=0.5) and CP scores greater than chance. In time series plots, the mean is depicted using circle data points in grey; mean smoothed data using a loess function is shown in solid (HbR) line. Confidence intervals are underlaid and shown in grey.

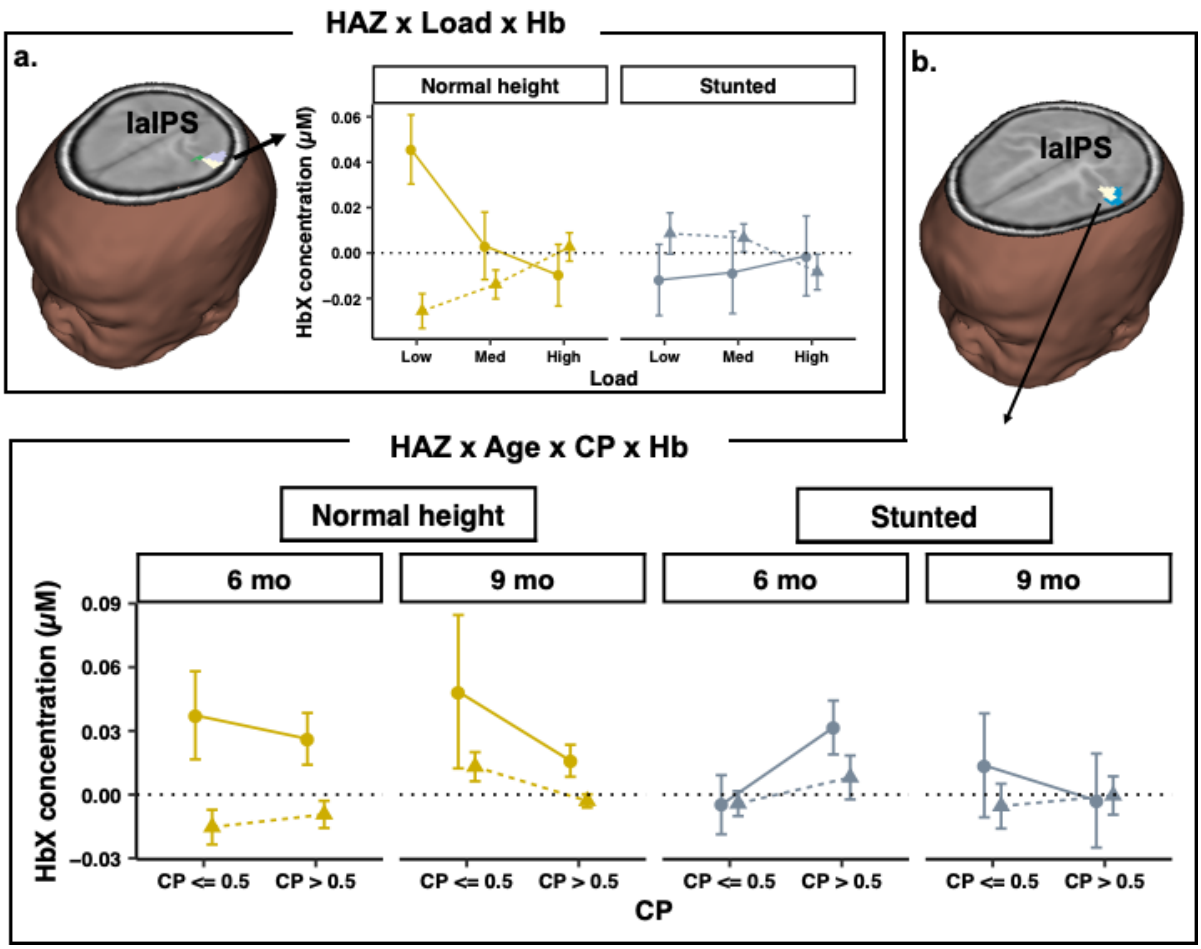

Figure 4. (a) Brain image shows location of interaction between HAZ, load and chromophore (lavender), interaction between age and chromophore (green cluster from Figure 3a) and overlap (white) in a superior cluster in laIPS. Right panel shows mean ± SE HbO (solid circles) and HbR (dashed triangles) concentration across the hemodynamic time window (0-20s) for normal height (yellow) and stunted (grey) infants at the low, medium, and high loads. (b) Brain image shows location of interaction between HAZ, age, CP score, and chromophore (white represents overlap between this interaction and main effect of chromophore) and main effect of chromophore (blue cluster from Figure 3a) in a superior cluster in laIPS. Note that the cluster for the interaction between HAZ, age, CP score and chromophore was subsumed by the overlap (shown in white). Bottom panel shows mean ± SE HbO (solid circles) and HbR (dashed triangles) concentration across the hemodynamic time window (0-20s) for normal height (yellow) and stunted (grey) 6-month-old and 9-month-old infants with CP scores less then chance (<=0.5) and CP scores greater than chance.

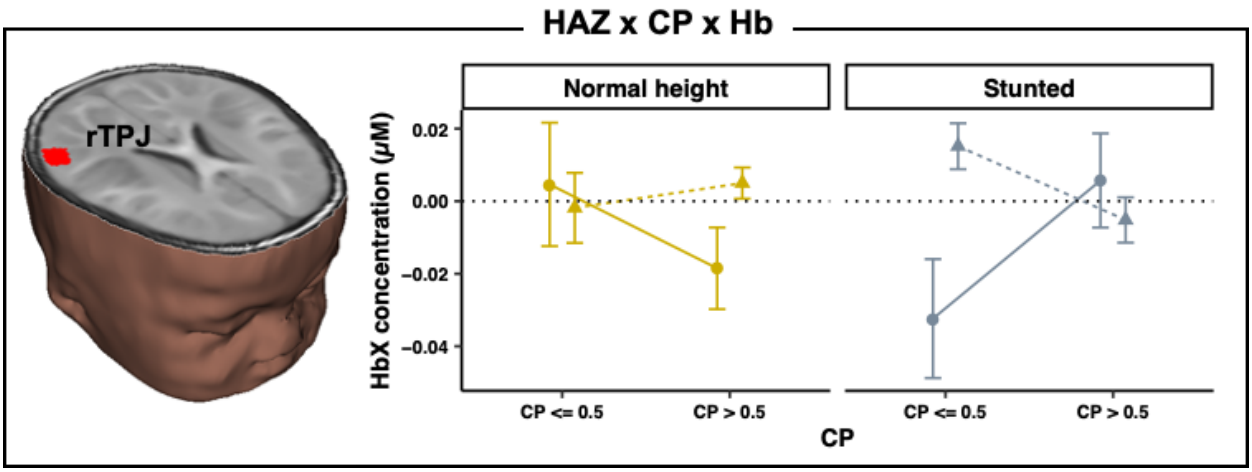

Figure 5. Brain image shows location of interaction between HAZ, CP score, and chromophore in rTPJ. Right panel shows mean ± SE HbO (solid circles) and HbR (dashed triangles) concentration across the hemodynamic time window (0-20s) for normal height (yellow) and stunted (grey) infants with CP scores less then chance (<=0.5) and CP scores greater than chance.

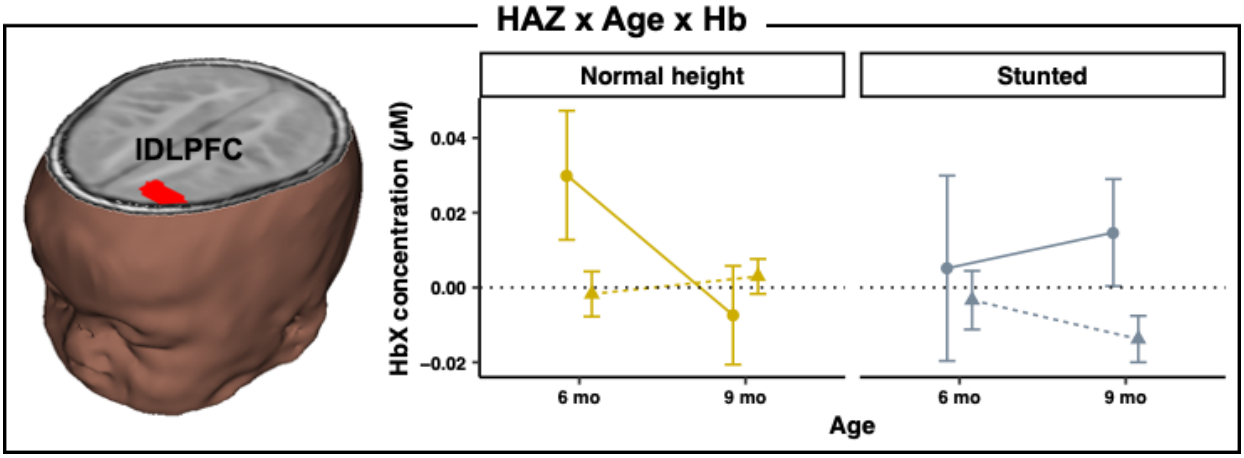

Figure 6. Brain image shows location of interaction between HAZ, age, and chromophore in lDLPFC. Right panel shows mean ± SE HbO (solid circles) and HbR (dashed triangles) concentration across the hemodynamic time window (0-20s) for 6-month-old and 9-month-old normal height (yellow) and stunted (grey) infants.

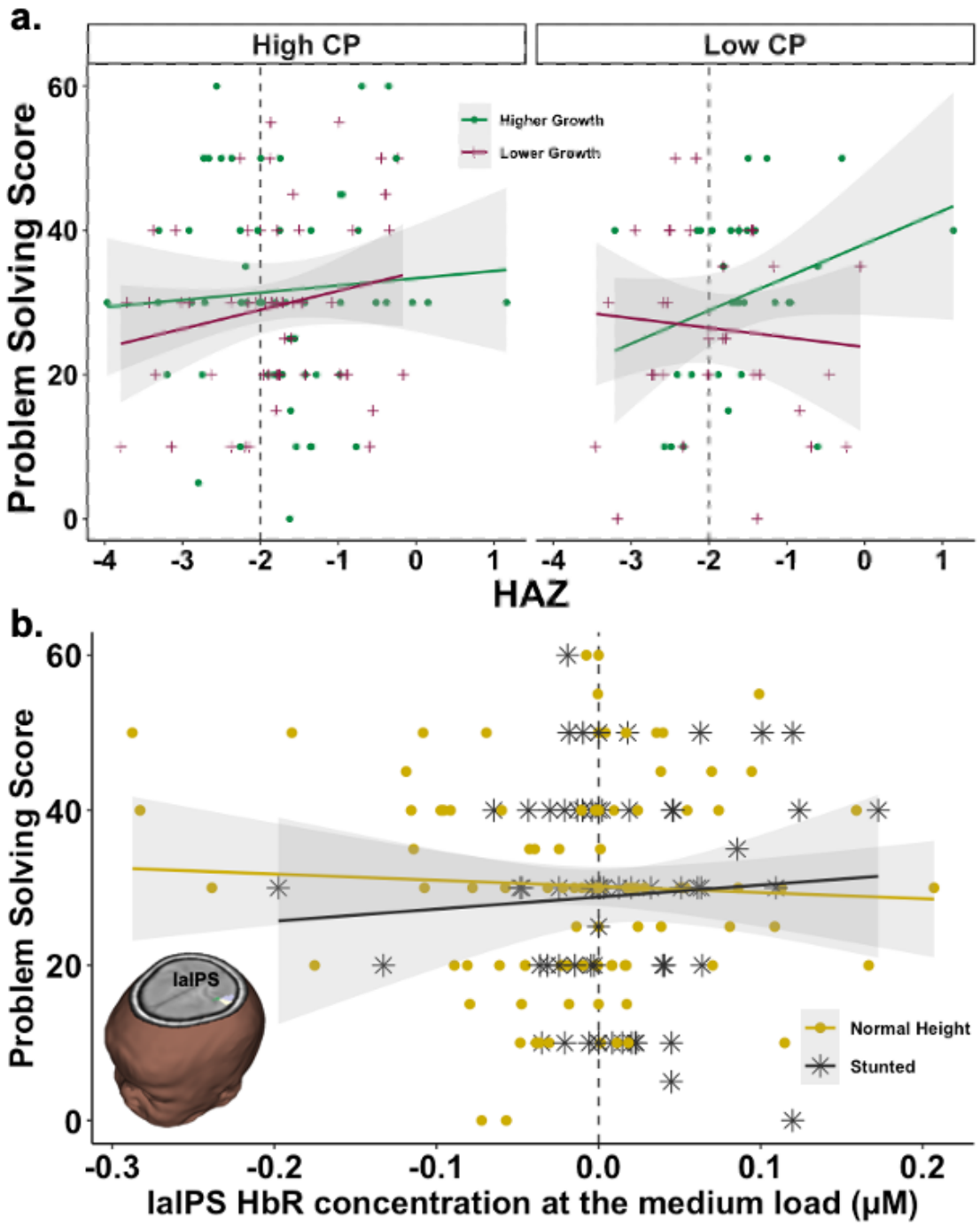

Figure 7. (a) Impact of HAZ and CP scores on problem-solving outcomes one year later. Infants with higher linear growth from year 1 to year 2 based on a median split are shown in green circles; infants with lower linear growth are shown in purple +. Left panel shows scatter plot with infants with higher CP scores in year 1 based on a median split, while right panel shows scatter plot with data from infants with lower CP scores in year 1. Vertical line shows typical stunting cut-off value (HAZ < -2). (b) Association between HAZ and laIPS HbR concentration from medium load in year 1 on problem-solving scores one year later. Normal height infants (HAZ >= -2) are shown in yellow circles; stunted infants (HAZ < -2) are shown in grey asterisks. Inset brain image shows location of the laIPS cluster (from Figure 4a).

Methods

Participants. Families with infants aged 6 months ± 15 days or 9 months ± 15 days from the villages in and around Shivgarh in the district of Raebarelli, Uttar Pradesh, India were contacted by researchers from the Community Empowerment Lab (CEL). Infants born to parents screened with colour vision deficits (due to the nature of the VWM task) or any congenital problems, or gestational age < 26 weeks at birth were excluded from the study. Infants were enrolled across four waves of data collection separated by 3 months from May 2017 to February 2018 (year 1). Approximately 30 6-month-olds and 30 9-month-olds were enrolled in each wave. Infants were also followed up for another year from 2018 to 2019 (year 2).

Across both years, each family participated in laboratory visits, home visits, and MRI visits. During the laboratory visit, physical growth measurements, behavioural and brain imaging (fNIRS) data, and cognitive assessment data were collected. During the home-visit, physical growth measurements were taken. During the MRI visit, physical growth measurements and anatomical scans were collected. If it was not possible to collect all the data in a single visit, the family was invited for multiple visits scheduled in close succession. The timeline of these visits were as follows: (1) a laboratory visit in 6 months (year 1) and 18 months (year 2) for the 6-month-old cohort, and at 9 months (year 1) and 21 months (year 2) for the 9-month-old cohort, (2) a home visit every three months thereafter in year 1 and year 2 (e.g., at 9, 12, 15, 21, 24 and 27 months for the 6-month-old cohort and at 12, 15, 18, 24, 27 and 30 months for the 9-month-old cohort), and (3) an MRI visit in year 1 (e.g., at 6 months for the 6-month-old cohort and 9 months for the 9-month-old cohort). Note that the assessments reported here were a subset of the full research protocol for the project. The full list of assessments can be found in the Supplementary materials.

277 families met the inclusion criteria and gave due consent. From this sample, 37 children did not complete the first in-take assessment (19 6-month-olds and 17 9-month-olds). The remaining 240 families were enrolled into the study. Data from 17 infants were excluded from all analyses due to problems with the behavioural and neuroimaging data collection and processing (not enough behavioural data in 9 infants, technical problems with the neuroimaging system for 7 infants, and neuroimaging data lost due to motion artifacts from 1 infant). We included infants in the analyses if they had usable fNIRS for at least one load of the VWM task. Data from 223 infants were included in the final analyses (see Supplementary Table 1 for demographic details on this sample). The study was approved by the Community Empowerment Lab Institutional Ethics Committee (Ref. No: CEL/2018005) in compliance with ethical regulations and standards. Some families also provided consent to use their images for knowledge and research purposes.

Materials and Procedure

General procedures for the laboratory visit. Families were transported in groups from their homes to the CEL Facility in Shivgarh. They were first escorted to the waiting room of the facility. Some groups of families were also provided a tour of the facility and a demonstration of the procedures to make them feel more comfortable and allow them to ask questions. Next, the families were escorted back to the waiting room where informed consent was sought. Participants' caregivers provided written informed consent; where caregivers were illiterate, a witness gave signed consent accompanied by a thumb impression of the caregiver in place of a signature. After consent was obtained, physical measurements of the infant were taken. The infant's head circumference was also measured to prepare an appropriately sized cap for fNIRS data collection.

Next, the parent and the infant were escorted to the fNIRS assessment room. The room was colored in a neutral grey to prevent distraction of the infant. The mother was seated on a chair and the infant was placed on the mother's lap approximately 100 cm away from the TV screen (see Fig. 1b). A cartoon was played on a TV screen to engage the infant. When the infant looked comfortable, two researchers placed an appropriately sized fNIRS cap on the head and fastened the chinstrap to hold it in place. After adjusting fNIRS signals (e.g., clearing hair from under individual fNIRS optodes), one researcher proceeded to use a Polhemus sensor to collect coordinates of the scalp landmarks and source and detector positions, while a second researcher placed a calibration sticker on the infant's forehead and set up the eye-tracker to record eye-movements from the infant. A 5-point calibration sequence was played on the monitor to ensure correct eye-tracking at the top, bottom, left, right and central parts of the screen.

After this, the VWM task was presented and video recordings, eye-tracking and fNIRS data collection ensued. If the infant showed signs of distress, cartoon clips were played in-between trials. Breaks were provided if the infant needed to be fed, fell asleep, or could not be calmed even after the use of the cartoon clips. The family was escorted back to the waiting room after the completion of the assessment or if the infant and/or mother needed a break from the assessment. In year 2, the mother and infant were escorted to another room to administer the ASQ assessment. At the end of each laboratory session, families received a small gift for participating in the study.

Physical growth measurements. Physical growth measurements were taken during laboratory visits, home visits, and MRI visits unless two or more visits were close in time, in which case, a single measurement was used for that time point. Measurements of head circumference, mid-upper arm circumference, calf circumference, infant's weight, and infant's length were taken by two members of the research team who were trained through a standardized workshop. Head circumference, mid-upper arm circumference, and calf circumference were measured twice using a SECA measurement tape. Measurements were repeated if there were any discrepancies of > 7 mm between two measurements. An infantometer was used for measuring the child's length from head to heel with 1 mm precision. A digital SECA weighing scale was used to measure the baby's weight with 10 grams precision.

VWM task. Infants were presented with a preferential looking VWM task[15] during the laboratory visit. A PC running *Experiment Builder* (SR Research) was used to present the task on a 42-inch LCD TV screen. Infants sat on their parents' lap approximately 100 cm away from the screen. Each stimulus display area was 29.5cm in width and 21cm in height, with a 21cm gap between the display on the left and right (each colored square was approximately 5cm x 5cm). The displays had a solid grey background. The colors of the squares presented on each display were selected from a set of nine colors: green (RGB: 0, 153, 0), brown (128, 64, 32), black (0, 0, 0), violet (128, 0, 128), cyan (128, 255, 255), yellow (255, 255, 0), blue (0, 0, 255), white (255, 255, 255), and red (255, 0, 0). On a display, the colors of the squares differed from each other, but colors could be repeated between the displays (i.e., the same color could appear on both displays). The positions of the squares on each display were randomly selected from a 3-by-3 grid of possible positions. Eye-movement data was recorded using an Eyelink 1000 Plus eye-tracker (SR research) operating in binocular mode with a sampling rate of 500 Hz. Additionally, one camera recorded a view of the infants' face, and another camera recorded the TV display. These video recordings were used to extract looking data when eye-tracking information was not available (due to technical problems, reflectance, poor lighting, loss of calibration).

Each trial started with a dynamic attention cue. Once the eye-tracker / experimenter detected that the infant was looking at the attention-getter, the task proceeded to the VWM displays. Each trial consisted of side-by-side displays of colored squares that appeared for 500 ms and disappeared for 250 ms for a trial duration of 10 seconds. Each trial was followed by a minimal inter-trial interval of 5s, however, this period was typically longer as the trial was not initiated until the infant looked at the display following the dynamic attention cue. On the 'unchanging' side, the colors of the squares remained the same across each flash, while on the 'changing' side, one square changed its color across each flash. Visual working memory load was manipulated by varying the number of squares on each side across trials (1, 2, or 3 squares on each side). The aim was to present each infant with 36 total trials in six blocks of 6 trials, although where the infant and parent were willing to continue, additional blocks were sometimes collected. Each block contained 2 trials for each load, one with the changing side on the left, one with the changing side on the right. Order of trials was randomized in each block. Where necessary, participants could take a break between blocks.

Functional near-infrared spectroscopy (fNIRS) data acquisition. fNIRS data was collected from infants as they engaged with the VWM task during the laboratory visit. A TechEn CW7 system (12 sources and 24 detectors) with wavelengths of 830 nm and 690 nm and sampling rate of 25 Hz was used. Fiber optic cables were used to carry light from the TechEn system to a cap with a customized probe geometry of 36 channels overlying the frontal, parietal, and temporal cortices (see Fig. 1c). A laptop connected to the fNIRS system recorded and displayed data as it was being collected. This laptop was also connected to the *Experiment Builder* computer to synchronize fNIRS data with the start of each trial of the task. A Polhemus Patriot Motion Sensor was used to digitize scalp landmarks and positions of sources and detectors on the cap.

MRI data acquisition. Anatomical data were collected on a Philips Achieva 3T MRI scanner equipped with 12-channel head RF array in an MRI Facility in Lucknow, India. The protocol used volumetric T_1-weighted SPGR acquisition. All imaging was performed during natural sleep[49]. Acquisition parameters were as follows: For T_1 SPGR: Field of View (FoV) = 19 x 19cm; slice thickness (ST) = 1.2 mm; acquisition matrix = 194 x 194; flip angle = 9º; echo time (TE) = 3.72 ms; repetition time (TR) = 9.5 ms; and receiver bandwidth (BW) = 270 Hz/voxel.

Ages-and-Stage Questionnaire III (ASQ) assessment. The ASQ was administered during laboratory visits in year 2 when the infants were 18 months (for the 6-month-old cohort) or 21 months (for the 9-month-old cohort). The appropriate ASQ questionnaire for each infant was selected using the online ASQ calculator (https://agesandstages.com/free-resources/asq-calculator/). While ASQ is designed as a screening questionnaire to be completed by parents, we adapted its administration to improve the reliability of the data. Specifically, a trained assessor administered the ASQ in collaboration with the parent. In cases where questions from the ASQ materials kit asked about behaviors that could be elicited in the laboratory (e.g., 'When you ask your child to, does he go into another room to find a familiar toy or object?'), these tasks were completed 'live', ensuring that the child was given ample time to perform each task. In the event the child was unable to perform the task, or the question was not amenable to live assessment, the mother's verbal report on the question was taken as the response. The ASQ yields five subscales of development: communication, gross motor, fine motor, problem-solving, and personal-social. Each subscale contained 6 questions, making up a total of 30 questions on the form. For this study,

we focused on the problem-solving scale as it was most directly related to VWM function, and we were interested in investigating later cognitive outcomes.

Methods of Analysis

Physical growth measurements analyses. A height-for-age z-score was calculated by dividing the difference between each infant's height and the age-specific height obtained from WHO growth standards by the age-specific standard deviation. Participants contributed between 1 and 11 observations for their height-for-age z-score across the study. On average, participants contributed 6.54 observations (*SD* = 1.92 observations), 83 days apart from each other (*SD* = 24.5 days). To obtain individual estimates of physical growth, a linear mixed effects model was run, taking height-for-age z-scores as the dependent variable, and participant age in days as an independent variable. As the trend was not perfectly linear, a quadratic transformation of age in days was also added to the model. Both age and age squared were orthogonal, that is, they were independently scaled and centered to avoid autocorrelation. The models had a random effect structure such that the intercept, the linear age term, and the quadratic age term were nested by participant. The random effect coefficients of the model were then extracted for each participant, such that each participant had an intercept term (HAZ), a linear age term (HAZ-L), and a quadratic term. As age in days was scaled and centered, the intercept term, used in most analyses, represents an area under the curve, rather than an initial estimate. HAZ scores were available for all 223 infants.

Measurements were also taken for weight adjusted z-score (WAZ), weight for length, arm circumference, and head circumference as well as the participants' body mass index (BMI). All of these, excluding BMI, were modelled in an identical fashion to the HAZ scores to extract individual coefficients. While all of these measurements share a certain amount of variance, HAZ was selected as the variable of interest as it had the highest correlation with socioeconomic status ($t(238) = 5.912$, $p < 0.001$, Pearson correlation = 0.358).

VWM task analyses. On average, infants completed 21.8 trials (*SD* = 10.2). SR research *Data Viewer* was used to export frame-by-frame eye-tracking data. The areas of interest around the two objects on the screen was modified such that the eye-tracking data would match video-coded data where the primary categories were 'left', 'right' and 'away'. Manually-coded data based on video recordings was used to replace trials where no eye-tracking information was available. *Datavyu* (https://datavyu.org/) was used to manually code these video recordings capturing the TV screen and the infant's face. A neutral observer coded the infant's eye-movements into 'left', 'right and 'away' looks for each frame for each trial. We computed reliability using Cohen's Kappa, a statistic that looks at percent agreement across categories normed by the base rate of each category. Kappa values from 0.6-0.8 indicate substantial reliability. Scores greater than 0.8 indicate almost perfect agreement. Overall, we coded 15% of the data to check reliabilities. Reliabilities were very good with a mean Kappa of 0.73 for the 6-month-old cohort and a mean Kappa of 0.83 for the 9-month-old cohort. Once coded, data were then exported in a format compatible with the eye-tracking data. The manually coded trials made up 31.9% of the total number of trials.

Data pre-processing was carried out using the R package *eyetrackingR*[50]. Two key measures were obtained from the data – total looking time (TLT) and change preference (CP). TLT for each trial was calculated as the sum of time spent looking at both displays. CP was calculated as the time spent looking at the changing side divided by the total looking to both

displays during a critical time window of between 1500 ms and 6500 ms for each trial (out of the 10000 ms trial window). The first 1500 ms comprised the first two flickers (2 * [250ms off and 500 ms on period]) was excluded to allow infants to explore the displays and, potentially, detect the changing and unchanging sides. The final 3500 ms was also excluded because the number of eye-tracking samples diminished as attention waned. Trials during which 75% of the data were coded as not looking at the displays were excluded from further analyses. Following these processing steps, out of the 223 children included in the analyses, 214 children contributed CP scores for load 1, 209 children contributed CP scores for load 2, and 214 children contributed CP scores for load 3.

A linear model with the CP score as the dependent variable and the age (6 or 9 months), load (1, 2, or 3), HAZ score, and TLT (in milliseconds) as independent variables was used to model the behavioural data. All interactions between independent variables were included. Participant SES status (measured using the Kuppuswamy scale[51]) and other related variables (e.g., nutrition information) were added in individually to assess whether there was an improvement to the model fit; however, these additional predictors were discarded as they either were colinear with HAZ or did not contribute substantially to model fit. An attempt was made to allow for the individual level variance by adding a random intercept for each participant, but this resulted in a singular fit, indicating the random effect was estimated at approximately zero.

fNIRS data pre-processing. For the fNIRS analyes, 221 children had fNIRS data for load 1 (out of the 223 infants), 220 children had fNIRS data for load 2, and 221 children had fNIRS data for load 3. fNIRS data were pre-processed using *EasyNIRS* in HOMER2[52]. Raw data was pruned using the *enPruneChannels* function (dRange = 1e+04 to 1e+07, SNRthresh = 1, SDrange = 0-45). An average of 29% of the channels across runs and infants were pruned/lost/rejected. Next, the *hmrIntensity2OD* function was used to convert data to optical density units. Motion artifacts were identified and corrected using targeted principal components analysis through the *hmrMotionCorrectPCArecurse* function (tMotion = 1.0, tMask = 1.0, StdevThresh = 50 and AmpThresh = 0.5, nSV = 0.97, maxIter=5). The corrected data were examined for uncorrected motion artifacts using the *hmrMotionArtifactByChannel* function (tMotion = 1.0, tMask = 1.0, StdevThresh = 50 and AmpThresh = 0.5). If these artifacts fell within -1 to 18 s of a trial, the associated trial onset trigger was removed from further data processing using the *enStimRejection* function. These criteria were set based on prior work examining motion processing algorithms in a development dataset[52]. An average of 6% of the trials across runs and infants were lost due to motion artifacts. These data were then band-pass filtered using the *hmrBandpassFilt* function with high-pass and low-pass cut-off frequencies of 0.016 and 0.5 Hz, respectively. The processed data were further analysed using Image Reconstruction techniques described below.

Note that these motion correction parameters were based on data from a VWM study with 3.5- to 4.5-year-old children. More recent analyses of infant fNIRS data[53,54] have recommended similar motion correction parameters with one notable difference: these studies suggest using StdevThresh = 15. This difference is not surprising as setting this parameter is time consuming and subjective[54]. To examine how this would impact our findings, we re-ran all analyses with StdevThresh = 15. Although findings from this re-analysis were consistent with our main results (see Supplementary materials), the lower value yielded very high data loss (mean data loss with StdevThresh of 50 = 6.19%; mean data loss with StdevThresh of 15 = 37.22%), particularly for stunted infants (mean data loss with StdevThresh of 15 = 41.2%). This is a very high percentage of data loss, raising questions about whether findings obtained from using this conservative

threshold is representative of individual and/or group-level estimates of brain function in at-risk infants. Given this, we discuss findings from using StdevThresh = 50 in the final analyses.

Creating head models for fNIRS analyses. To create a head model for each infant, we used the anatomical MRI scan if it was available. Out of the 223 children included in the analyses, anatomical T1-weighted images were available for 72 6-month-old infants and 70 9-month-old infants. The remaining infants did not have an anatomical scan (45 6-month-olds and 36 9-month-olds). If a scan was not available, we used an age-specific MRI template. A 6-month-old template and a 9-month-old template were created from the available scans of 15 boys and 15 girls for each specific age, using a multistep registration procedure[55]. This procedure was carried out using *antsMultivariateTemplateConstruction2* provided by ANTS 2.1. Briefly, all the images were linearly aligned and averaged to provide a template estimate. Then, all images were nonlinearly aligned to this initial estimate. The results were averaged to provide an improved estimate. This process was repeated ten times to construct the final estimate. The 6-month-old template was used for the 45 6-month-olds who did not have anatomical scans and the 9-month-old template was used for the 36 9-month-old infants who did not have anatomical scans.

Next, head models were created from the anatomical scans and age-specific templates using tools available in AFNI (https://afni.nimh.nih.gov). We describe this briefly below. First, images were rotated using the *3dRotate* such that the nose was rotated towards the y-axis of the MRI scanner. The images were then resampled into a standard right-axial-superior orientation using *3dResample*. If large variations in signal quality were present in the image, *3dUnifize* was used to do bias field correction. The image was put into anterior commissure (AC) - posterior commissure (PC) alignment. To do this, a brain mask was created, and the brain was extracted from the image and aligned using the *auto_tlrc* function. The rigid body transform from the resulting transform was then used to reorient the image and brain mask into AC-PC alignment. The image was segmented into gray matter, white matter, and CSF using *3dSeg*. A corresponding model representing the outer surface of the scalp was generated by estimating the optimal threshold between the background air and the foreground head using *3dClipLevel*. This threshold was then applied to the image and holes in the resulting mask were filled using *3dinfill*. This segmentation representing the head was combined with the brain segmentation to generate a label map that contained four labels: gray matter, white matter, CSF, and a combination of skull and scalp. These head volume images were used for fNIRS Image reconstruction analyses described below.

Generating forward models and fNIRS Image Reconstruction. Details of the methodological pipeline used for image reconstruction are presented elsewhere[56]. We outline the steps below. First, we corrected for variations in scalp landmarks and positions of sources and detectors during digitization (for e.g., infant movement) using a three-step method in the *digitizeR* package. This method sequentially compares and aligns user-specified Euclidean distances between sources and detectors for an individual probe geometry with available templates for specific cap sizes. Head volumes created from segmenting the T1-weighted anatomical scans or age-specific templates were imported into *AtlasViewerGUI* in HOMER2[30,57]. Each infant's digitized scalp landmarks and probe geometry was projected onto each head volume. Monte Carlo simulations were run with 100 million photons to generate sensitivity profiles for each channel and wavelength. The head volume and sensitivity profiles were converted to NIFTII images. Next, image reconstruction techniques employing NeuroDOT tools[56,58] were used to integrate the head volume and sensitivity profiles with the processed fNIRS data to obtain voxel-wise relative changes in oxygenated (HbO) and de-oxygenated (HbR) concentrations.

A general linear model with three regressors (loads 1, 2, 3) was separately run for each chromophore and infant. We used a hemodynamic response function derived from DOT data for HbO and HbR data[56]. Each trial was modelled with a 10 s boxcar and variable inter-trial intervals. The inter-trial interval was a minimum of 5 s but could be typically longer as the trial was not initiated until the infant looked at the display following the dynamic attention cue. To control for the variability in the number of trials per condition and infant, we computed a weighted average of beta coefficient images per load, chromophore, and infant.

Registration to overall study template. The image-based fNIRS beta coefficient images from all infants were aligned to the same space by using an overall study template. This overall study template was created by repeating the same process described in the multistep registration procedure[55], using each age-specific template (6-month-old, 9-month-old, 12-month-old, 15-month-old, 18-month-old, 24-month-old, and 30-month-old)[59] - see 'Creating head models for fNIRS analyses' section above). For the current study, we used this overall study template, instead of a template generated from combining only the 6-month-old and 9-month-old templates, to provide consistency across current and future investigations on this project.

Group analyses. For group analyses, only voxels that contained data from 70% of the infants were included. To achieve this, the beta coefficient map for each condition, chromophore, and infant was masked and summed together to create one image. Only those voxels that contained at least 70% data were extracted to create the group mask. This group mask was used in the model below.

For Group analyses, the co-registered beta coefficient maps were entered into a linear mixed effects model using *3dLME* in AFNI with load (1, 2, 3), chromophore (HbO and HbR) and age (6-month-olds and 9-month-olds) as within-subject factors and CP and HAZ as quantitative predictors. For children who did not have a CP score at a load, an average CP score was calculated for that load from age-matched, gender-matched, and SES-matched infants. An average CP score was used for 9 infants for load 1, 14 infants for load 2, and 9 infants for load 3. After running the linear mixed effects model, *3dFWHM* was used to estimate the empirical auto-correlation function in our data and fit a mixed auto-correlation function model to this function. *3dClustSum* was run on the group brain mask with a voxelwise p threshold of .01, alpha threshold of .05, 10,000 iterations, 2-sided thresholding, first nearest-neighbour clustering, and with a minimum cluster size of 278 voxels. *3dClusterize* was used to threshold the main effect and interaction effect images. Average beta values were extracted from the thresholded clusters using *3dROIstats* in AFNI. Labels for significant clusters of activation were created based on regions of interest (ROIs) from VWM fMRI studies[30]. These ROIs in MNI space were co-registered to align with the overall study template. To assign a label to each significant cluster, Euclidean distances were calculated between the centre of mass of each ROI and each significant cluster. The ROI with the minimum distance to a cluster was used as the label. The range of distances between each cluster and final assigned label were 7.5 mm to 22.7 mm.

ASQ assessment analyses. Out of 223 children included in the analyses, 172 children had scores for the ASQ assessment. The rest of the families did not complete the assessment due to illness, non-attendance, or other factors. Non-standardized scores from the ASQ were used as there are no standardized norms for children from rural India. To examine whether behavioural performance in year 1 was related to the problem-solving score in year 2, we ran a linear model with the problem-solving score as the dependent variable, and CP scores, HAZ scores, and HAZ-L as

predictors. We included HAZ-L because change in physical growth over time was expected to be an important contributor to problem-solving score measured in year 2.

To examine whether brain function in year 1 was related to cognitive outcomes in year 2, we ran 6 linear models – one per chromophore (HbO and HbR) and load (1, 2, 3) for the laIPS cluster from the interaction between HAZ, load and chromophore. In each model, the dependent variable was problem-solving score, and the independent variable was laIPS activation. We also included the HAZ score as a predictor since laIPS activation was associated with HAZ. Note that we tested whether HAZ-L contributed significantly to these models; this was not the case, so this term was excluded from the final models. All models were checked with a Q-Q plot of the residuals and using the DHARMa[60] package v0.4.3 in R. As there was some level of dispersion in the data, models were run using robust regression (using the *robustbase* package in R) and model outliers were also checked using Cook's distance, indicating no problematic outliers.

Acknowledgements and funding sources.

This work was supported by Grant No. OPP1164153 from the Bill and Melinda Gates Foundation and Grant No. R01HD083287 from the National Institutes of Health awarded to J. P. Spencer, Grant No. RPG-2019-286 from the Leverhulme Trust awarded to S. Wijeakumar, and NIH Grant P50HD103556 awarded to V.A. Magnotta. We are grateful to the families from Shivgarh, Uttar Pradesh, India, for generously contributing their time for the study. We appreciate the efforts of the study team towards the high-quality and seamless conduct of this study. We thank Dr. Vishwajeet Kumar for his support and guidance throughout the project.

Author contributions.

JPS, SW and AK conceptualized the study. SW, SF, JPS, VAM, SD contributed to the methodology and software. SW, SF, JPS, VAM, KJ and SD contributed to formal analyses. VPS and MT contributed to project administration. SW, JPS and AK supervised the study. All authors contributed to the writing, review and editing processes.

Data availability

All final data used in statistical analyses will be publicly available on Github following publication. All raw and processed fNIRS data will be available by agreement through the Bill & Melinda Gates Foundation fNIRS Consortium hosted by Yale University/Haskins Laboratory.

Code availability

fNIRS analyses pipeline is publicly available under https://github.com/developmentaldynamicslab/MRI-NIRS_Pipeline. All code and revisions will be publicly available on Github following publication.

References

1. Adair, L. S. *et al.* Associations of linear growth and relative weight gain during early life with adult health and human capital in countries of low and middle income: findings from five birth cohort studies. *Lancet (London, England)* **382**, 525–534 (2013).
2. Walker, S. P., Chang, S. M., Powell, C. A. & Grantham-McGregor, S. M. Effects of early

childhood psychosocial stimulation and nutritional supplementation on cognition and education in growth-stunted Jamaican children: Prospective cohort study. *Lancet* **366**, 1804–1807 (2005).
3. Grantham-McGregor, S. *et al.* Developmental potential in the first 5 years for children in developing countries. *Lancet* **369**, 60–70 (2007).
4. *Repositioning Nutrition as Central to Development*. *Directions in Development - General* (The World Bank, 2005). doi:doi:10.1596/978-0-8213-6399-7.
5. Fink, G. *et al.* Schooling and wage income losses due to early-childhood growth faltering in developing countries: national, regional, and global estimates. *Am. J. Clin. Nutr.* **104**, 104–112 (2016).
6. Sudfeld, C. R. *et al.* Linear Growth and Child Development in Low- and Middle-Income Countries: A Meta-Analysis. *Pediatrics* **135**, e1266–e1275 (2015).
7. Xie, W. *et al.* Growth faltering is associated with altered brain functional connectivity and cognitive outcomes in urban Bangladeshi children exposed to early adversity. *BMC Med.* **17**, 199 (2019).
8. Fernandez-Baizan, C. *et al.* Development of visuospatial memory in preterm infants: A new paradigm to assess short-term and working memory. *Child Neuropsychol.* **27**, 296–316 (2021).
9. Clerkin, E. M., Hart, E., Rehg, J. M., Yu, C. & Smith, L. B. Real-world visual statistics and infants' first-learned object names. *Philos. Trans. R. Soc. B Biol. Sci.* **372**, (2017).
10. Cochrane, A., Simmering, V. & Green, C. S. Fluid intelligence is related to capacity in memory as well as attention: Evidence from middle childhood and adulthood. *PLoS One* **14**, e0221353–e0221353 (2019).
11. Alloway, T. P. & Alloway, R. G. Investigating the predictive roles of working memory and IQ in academic attainment. *J. Exp. Child Psychol.* (2010) doi:10.1016/j.jecp.2009.11.003.
12. Davidson, C., Shing, Y. L., McKay, C., Rafetseder, E. & Wijeakumar, S. The first year in formal schooling improves working memory and academic abilities. *Dev. Cogn. Neurosci.* **60**, 101205 (2023).
13. Nevo, E. & Bar-Kochva, I. The Relations Between Early Working Memory Abilities and Later Developing Reading Skills: A Longitudinal Study From Kindergarten to Fifth Grade. *Mind, Brain, Educ.* **9**, 154–163 (2015).
14. Bull, R., Espy, K. A. & Wiebe, S. A. Short-term memory, working memory, and executive functioning in preschoolers: Longitudinal predictors of mathematical achievement at age 7 years. *Dev. Neuropsychol.* (2008) doi:10.1080/87565640801982312.
15. Ross-Sheehy, S., Oakes, L. M. & Luck, S. J. The Development of Visual Short-Term Memory Capacity in Infants. *Child Dev.* (2003) doi:10.1046/j.1467-8624.2003.00639.x.
16. Delgado Reyes, L., Wijeakumar, S., Magnotta, V. A., Forbes, S. H. & Spencer, J. P. The functional brain networks that underlie visual working memory in the first two years of life. *Neuroimage* **219**, 116971 (2020).
17. Wijeakumar, S., Kumar, A., M. Delgado Reyes, L., Tiwari, M. & Spencer, J. P. Early adversity in rural India impacts the brain networks underlying visual working memory. *Dev. Sci.* (2019) doi:10.1111/desc.12822.
18. Kwon, M. K., Luck, S. J. & Oakes, L. M. Visual Short-Term Memory for Complex Objects in 6- and 8-Month-Old Infants. *Child Dev.* **85**, 564–577 (2014).
19. Oakes, L. M., Hurley, K. B., Ross-Sheehy, S. & Luck, S. J. Developmental changes in

infants' visual short-term memory for location. *Cognition* vol. 118 293–305 (2011).
20. Todd, J. J., Fougnie, D. & Marois, R. Visual short-term memory load suppresses temporo-parietal junction activity and induces inattentional blindness. *Psychol. Sci.* **16**, 965–972 (2005).
21. Corbetta, M. & Shulman, G. L. Control of goal-directed and stimulus-driven attention in the brain. *Nat. Rev. Neurosci.* **3**, 201–215 (2002).
22. Todd, J. J. & Marois, R. Capacity limit of visual short-term memory in human posterior parietal cortex. *Nature* (2004) doi:10.1038/nature02466.
23. Todd, J. J. & Marois, R. Posterior parietal cortex activity predicts individual differences in visual short-term memory capacity. *Cogn. Affect. Behav. Neurosci.* (2005) doi:10.3758/CABN.5.2.144.
24. Hemalatha, R. *et al.* Mapping of variations in child stunting, wasting and underweight within the states of India: the Global Burden of Disease Study 2000–2017. *eClinicalMedicine* **22**, (2020).
25. Cosman, J. D., Lowe, K. A., Zinke, W., Woodman, G. F. & Schall, J. D. Prefrontal Control of Visual Distraction. *Curr. Biol.* **28**, 414-420.e3 (2018).
26. Ellis, C. T., Skalaban, L. J., Yates, T. S. & Turk-Browne, N. B. Attention recruits frontal cortex in human infants. *Proc. Natl. Acad. Sci.* **118**, e2021474118 (2021).
27. Posner, M. I., Rothbart, M. K., Sheese, B. E. & Voelker, P. Control networks and neuromodulators of early development. *Developmental Psychology* vol. 48 827–835 (2012).
28. Delgado Reyes, L., Wijeakumar, S., Magnotta, V. A., Forbes, S. H. & Spencer, J. P. The functional brain networks that underlie visual working memory in the first two years of life. *Neuroimage* **219**, 116971 (2020).
29. Edin, F. *et al.* Mechanism for top-down control of working memory capacity. *Proc. Natl. Acad. Sci. U. S. A.* **106**, 6802–6807 (2009).
30. Wijeakumar, S., Spencer, J. P., Bohache, K., Boas, D. A. & Magnotta, V. A. Validating a new methodology for optical probe design and image registration in fNIRS studies. *Neuroimage* **106**, 86–100 (2015).
31. Vossel, S., Geng, J. J. & Fink, G. R. Dorsal and ventral attention systems: Distinct neural circuits but collaborative roles. *Neuroscientist* **20**, 150–159 (2014).
32. Olesen, P. J., Macoveanu, J., Tegnér, J. & Klingberg, T. Brain activity related to working memory and distraction in children and adults. *Cereb. Cortex* **17**, 1047–1054 (2007).
33. McKay, C. A., Shing, Y. L., Rafetseder, E. & Wijeakumar, S. Home assessment of visual working memory in pre-schoolers reveals associations between behaviour, brain activation and parent reports of life stress. *Dev. Sci.* (2021) doi:10.1111/desc.13094.
34. Thomason, M. E. *et al.* Development of spatial and verbal working memory capacity in the human brain. *J. Cogn. Neurosci.* **21**, 316–332 (2009).
35. Arredondo, M. M., Aslin, R. N. & Werker, J. F. Bilingualism alters infants' cortical organization for attentional orienting mechanisms. *Dev. Sci.* **25**, e13172 (2022).
36. Buss, A. T., Fox, N., Boas, D. A. & Spencer, J. P. Probing the early development of visual working memory capacity with functional near-infrared spectroscopy. *Neuroimage* (2014) doi:10.1016/j.neuroimage.2013.05.034.
37. Wijeakumar, S., Magnotta, V. A. & Spencer, J. P. Modulating perceptual complexity and load reveals degradation of the visual working memory network in ageing. *Neuroimage* (2017) doi:10.1016/j.neuroimage.2017.06.019.

38. Todd, J. J. & Marois, R. Capacity limit of visual short-term memory in human posterior parietal cortex. *Nature* **428**, 751–754 (2004).
39. Ambrose, J. P., Wijeakumar, S., Buss, A. T. & Spencer, J. P. Feature-based change detection reveals inconsistent individual differences in visual working memory capacity. *Front. Syst. Neurosci.* (2016) doi:10.3389/fnsys.2016.00033.
40. Spencer, J. P. *et al.* Poor air quality is associated with impaired visual cognition in the first two years of life: A longitudinal investigation. *Elife* **12**, (2023).
41. Corbetta, M., Patel, G. & Shulman, G. L. The Reorienting System of the Human Brain: From Environment to Theory of Mind. *Neuron* **58**, 306–324 (2008).
42. Corbetta, M., Kincade, J. M., Ollinger, J. M., McAvoy, M. P. & Shulman, G. L. Voluntary orienting is dissociated from target detection in human posterior parietal cortex. *Nat. Neurosci.* **3**, 292–297 (2000).
43. Rose, S. A., Feldman, J. F. & Jankowski, J. J. Implications of Infant Cognition for Executive Functions at Age 11. *Psychol. Sci.* **23**, 1345–1355 (2012).
44. Jensen, S. K. G., Berens, A. E. & Nelson, C. A. Effects of poverty on interacting biological systems underlying child development. *Lancet Child Adolesc. Heal.* **1**, 225–239 (2017).
45. Kar, B. R., Rao, S. L. & Chandramouli, B. A. Cognitive development in children with chronic protein energy malnutrition. *Behav. Brain Funct.* **4**, 1–12 (2008).
46. Perdue, K. L. *et al.* Using functional near-infrared spectroscopy to assess social information processing in poor urban Bangladeshi infants and toddlers. *Dev. Sci.* **22**, e12839 (2019).
47. Lloyd-Fox, S. *et al.* Habituation and novelty detection fNIRS brain responses in 5- and 8-month-old infants: The Gambia and UK. *Dev. Sci.* **22**, e12817 (2019).
48. Landry, S. H., Smith, K. E., Swank, P. R. & Guttentag, C. A responsive parenting intervention: the optimal timing across early childhood for impacting maternal behaviors and child outcomes. *Dev. Psychol.* **44**, 1335–1353 (2008).
49. Dean 3rd, D. C. *et al.* Modeling healthy male white matter and myelin development: 3 through 60months of age. *Neuroimage* **84**, 742–752 (2014).
50. Dink, J. W. & Ferguson, B. (2015). eyetrackingR: An R Library for Eye-tracking Data Analysis.
51. Shaikh, Z. & Pathak, R. Revised Kuppuswamy and B G Prasad socio-economic scales for 2016. *Int. J. Community Med. Public Heal.* **4**, 997 (2017).
52. Reyes, L. M. D., Bohache, K., Wijeakumar, S. & Spencer, J. P. Evaluating motion processing algorithms for use with functional near-infrared spectroscopy data from young children. *Neurophotonics* **5**, 25008 (2018).
53. Gemignani, J. & Gervain, J. Comparing different pre-processing routines for infant fNIRS data. *Dev. Cogn. Neurosci.* **48**, 100943 (2021).
54. Di Lorenzo, R. *et al.* Recommendations for motion correction of infant fNIRS data applicable to multiple data sets and acquisition systems. *Neuroimage* **200**, 511–527 (2019).
55. O'Muircheartaigh, J. *et al.* White matter development and early cognition in babies and toddlers. *Hum. Brain Mapp.* **35**, 4475–4487 (2014).
56. Forbes, S. H., Wijeakumar, S., Eggebrecht, A., Magnotta, V. & Spencer, J. P. A processing pipeline for image reconstructed fNIRS analysis using both MRI templates and individual anatomy. *Neurophotonics*.

57. Aasted, C. M. *et al.* Anatomical guidance for functional near-infrared spectroscopy: AtlasViewer tutorial. *Neurophotonics* **2**, 20801 (2015).
58. Eggebrecht, A. T. *et al.* Mapping distributed brain function and networks with diffuse optical tomography. *Nat. Photonics* **8**, 448–454 (2014).
59. Lancaster, J. L. *et al.* Bias between MNI and talairach coordinates analyzed using the ICBM-152 brain template. *Hum. Brain Mapp.* **28**, 1194–1205 (2007).
60. Hartig, F. DHARMa: Residual Diagnostics for Hierarchical (Multi-Level / Mixed) Regression Models. R package version 0.4.5. (2022).

1012